https://doi.org/10.3311/PPci.21359

Periodica Polytechnica Civil Engineering, 68(1), pp. 37–56, 2024

The Modified Energy-based Method for Seismic Evaluation of Structural Systems with Different Hardening Ratios and Deterioration Hysteresis Models

Rasool Nodeh Farahani[1], Gholamreza Abdollahzadeh[1*], Alireza Mirza Goltabar Roshan[1]

[1] Department of Civil Engineering, Faculty of Structural and Earthquake Engineering, Babol Noshirvani University of Technology, Shariati Avenue, Babol, 47148-71167, Mazandaran, Iran
[*] Corresponding author, e-mail: abdollahzadeh@nit.ac.ir

Received: 17 October 2022, Accepted: 23 July 2023, Published online: 17 August 2023

Abstract

Prediction of target displacement in structural systems plays a significant role in performance-based design and rehabilitation of structures. In this study, the *γ* factor for different hardening ratios, including 1, 2, 3, 5, 7.5, 10, and 15 percentages, stiffness-strength-deterioration models, and soil type classes is determined to modify the energy balance equation in performance-based plastic design (PBPD). Statistical results indicate that the effect of the hardening ratio, deterioration, and soil type class on the capacity curve is considerable. Therefore, a simple equation based on the period of the vibration and ductility is suggested to estimate the *γ* factor in different structural systems. Moreover, four 1-, 3-, 7-, and 12-story moment steel structures with various hardening ratios in the material are designed to validate the proposed method. The suggested values for the *γ* factor show exact results compared to collected displacements from time history analysis, while the error in the previous work was considerable. Statistical results showed that the mean error in the previous method in estimating target displacement for 1-, 3-. 7-, and 12-story structures is about 15%, 20%, 20%, and 32%, respectively. Conversely, the mean error in this study for estimating target displacement of 1-, 3-. 7-, and 12-story structures is about 10%, 7%, 6%, and 15%, respectively. Finally, the proposed method is examined on the empirical reinforced concrete (RC) bridge pier simulated numerically with fiber-based modeling. Similarly, the suggested equation estimates the target displacement appropriately for the concrete model compared to achieved displacements from nonlinear dynamic analysis.

Keywords

gamma factor, hardening ratio, deterioration, soil class, target displacement

1 Introduction

Over the years, different methods for predicting structural demand under desired seismic hazard levels have been proposed, such as the coefficient method [1], capacity spectrum method [2], N_2 method [3, 4], energy balance concept [5–11], and the other ones. Based on the coefficient method, the linear elastic response of the single-degree-of-freedom (SDOF) system by multiplying a series of coefficients to estimate target displacement [12]. The mentioned method was developed firstly by Veletsos and his colleagues [13, 14] and comprehensively extended by Miranda [15–17], Baez and Miranda [18] and Ruiz-García and Miranda [19]. According to the capacity spectrum method, the maximum nonlinear displacement of the SDOF structure is estimated by the equivalent linear system using an effective period of vibration (T_{eff}) and damping (ξ_{eff}) [20–22]. Based on the N2 method, the maximum global displacement of the SDOF system is estimated based on the intersection of the capacity pushover curve (V_b–D_t converted to S_a–S_d) in AD format with demand curve (standard acceleration curve) in different ductility ranges. The energy balance concept was used initially by Veletsos and Newmark [14], Veletsos et al. [13], and Newmark and Hall [23] to determine nonlinear response spectra in different ductility ranges by using elastic-perfectly-plastic hysteresis model, reference to Fig. 1. The mentioned method was perfectly developed by Goel and his colleagues [5–9] by the intersection of energy demand and energy capacity for estimating maximum target displacement. They used the energy balance concept based on the theory of the input energy where the energy needed to push a system monotonically up to maximum target displacement is equal to the maximum

Cite this article as: Farahani, R. N., Abdollahzadeh G., Roshan, A. M. G. "The Modified Energy-based Method for Seismic Evaluation of Structural Systems with Different Hardening Ratios and Deterioration Hysteresis Models", Periodica Polytechnica Civil Engineering, 68(1), pp. 37–56, 2024. https://doi.org/10.3311/PPci.21359

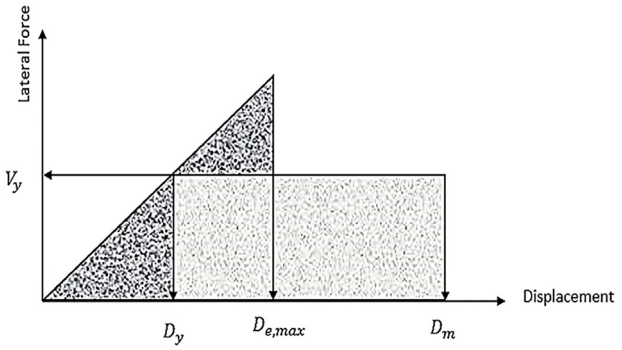

Fig. 1 Energy balance concept

earthquake input energy for equivalent elastic systems, approximated by $E = 1/2\ mS_v^2$ equation (m is mass, S_v is pseudo velocity). The mentioned theory was confirmed by several researchers.

Although structural systems under strong ground motion shaking illustrate uncontrollable and unpredictable structural damage [24], predicting target displacement for initial evaluation of component status in structural elements and predicting probable behavior of them in future earthquakes plays a significant role in performance-based plastic design and rehabilitation of buildings. The energy balance concept has been developed for predicting target displacement in structural systems based on the assumption that the energy computed from the monotonic load (capacity spectrum) is equal to input energy produced by earthquake ground motions. As illustrated in Fig. 1, the energy balance equation can be written by the given equation [9]:

$$E = \frac{1}{2} m s_v^2 = \frac{1}{2} V_y D_y + V_y \left(D_m - D_y \right), \tag{1}$$

where m is the structural mass, s_v is the pseudo-velocity, V_y is the yield strength of the system, D_y is the yield displacement of the system, and D_m is the maximum displacement in the system.

The explained energy-balance equation was only valid for structural systems with periods in the acceleration-sensitive region [6]. Therefore, Lee and Goel [5] introduced the Gamma factor (γ) to modify the energy balance equation for estimating target displacement. The energy balance equation was modified as given [9]:

$$\gamma E = \gamma \frac{1}{2} m s_v^2 = \frac{1}{2} V_y D_y + V_y \left(D_m - D_y \right), \tag{2}$$

$$\gamma = \frac{\frac{1}{2} V_y D_y + V_y \left(D_m - D_y \right)}{\frac{1}{2} m s_v^2} = \frac{\frac{1}{2} V_y D_y + V_y \left(D_m - D_y \right)}{\frac{1}{2} V_y D_y R_y^2} = \frac{2\mu - 1}{R_y^2} \tag{3}$$

where m is structural mass, s_v is the pseudo-velocity, V_y is the yield strength of the system, D_y is the yield displacement of the system, D_m is the maximum displacement in the system, R_y is the strength reduction factor, and μ is the ductility of the system (D_m / D_y).

The performance-based energy method has been popularly developed by several researchers for different purposes. For example, Zhang et al. [25] quantify the seismic demands of tension-only concentrically braced steel beam-through frames (TCBSBFs) under near-fault ground motions, or Ke et al. [26] developed the energy factor (γ) for self-centering, MRF (steel moment resisting frame) with fuses [27], and hybrid systems [28]. Wang et al. [29] proposed the energy factor based on the modified Clough hysteretic model in different constant-ductility levels. Due to the popularity of the mentioned theory in performance-based plastic design (PBPD) methodology, developing the cited procedure would be necessary for future investigations. The presented Gamma factor (γ) in the literature was only used for bi-linear systems, while it can be developed for systems with different hardening ratios. The hardening in most structural systems, especially steel structures, can be altered from 1% to higher percentages, such as multiplanar CHS X-connections [30, 31]. Moreover, the effect of soil type classes with different shear wave velocities has not been discussed before on this parameter. The influence of soil type class on the R-factor was confirmed by various researchers, such as Miranda [16] and Ruiz-García and Miranda [32], Rahnama and Krawinkler [33], and others. Hence, the Gamma factor (γ) would be affected by soil site conditions due to the dependent on the R-factor. Moreover, stiffness deterioration and strength degradation in structural systems are effective on displacement demand of the system under probable future events. The different stiffness deterioration and strength degradation protocols have not been considered before on Gamma factor (γ), where many researchers have confirmed its significant effect on seismic responses, such as Amirchoupani et al. [34, 35], Abdollahzadeh et al. [36], ASCE/SEI 41-17 [1], and FEMA series [37, 38].

According to the literature review, the Gamma factor (γ) in different hardening ratios, soil classes, and deterioration hysteresis models, including Modified Clough (MC), moderate-stiffness-strength-deterioration (MSD), and severe-stiffness-strength-deterioration (SSD), is developed to use in the energy balance equation and predicting target displacement in this study. It is worth mentioning that seven hardening ratios were considered in this investigation,

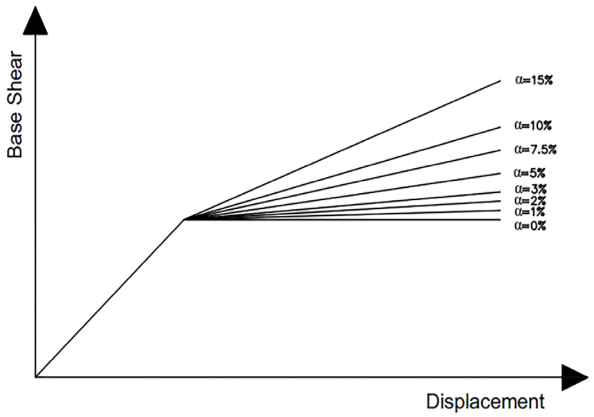

Fig. 2 Different hardening ratios

including 1, 2, 3, 5, 7.5, 10, and 15 percentages (Fig. 2). Then, a simple equation based on the ductility and period of vibration was suggested for estimating the γ factor. Finally, four steel moment structural systems with 1-, 3-, 7-, and 12-stories and one empirical RC bridge pier were employed to verify the proposed procedure and compared with the result of previous studies.

2 Methodology

In the first step, 210 earthquake ground motions were selected based on soil classes A, B, C, and D in this study. All earthquake records were chosen from NGA-West2 PEER ground motions. Therefore, three ground motion sets with shear wave velocity of 750 to 1500 (m/s^2), 365 to 750 (m/s^2), and 185 to 365 (m/s^2) based on ASCE/SEI 7 [39] soil classification was determined as shown in Table A1 to Table A3 in Appendix A, respectively. The magnitude of selected earthquakes is from 5.6 to 7.6 at shallow crustal tectonic shells and the 1-to-100-kilometer rapture distance. It is worth mentioning that the conditional mean spectrum (CMS) methodology based on Baker and Lee's [40] study was used to select earthquake ground motions for more compatibility and better spectral matching between ground motions. In this investigation, the OpenSEES version 3.0.3 and MATLAB 2020 software were used for dynamic time history analysis and post-processing of results, respectively. The zero-length element and mass-proportional Raleigh damping were adopted for SDOF modeling of mass-spring and damping, respectively. It is worth mentioning that the uniaxial *Material ElasticPP* and *Steel01* from the OpenSEES library was assigned to zero-length element to model the hysteresis behavior of the steel structures as an accepted method by many researchers and specifications [17, 34, 36, 38, 41]. Additionally, 30 periods of vibration from 0.1 s to 3 s with 0.1 s time intervals were considered for dynamic analysis. The system stiffness and yield displacement, with the 5% damping coefficient, were calculated in each period of vibration. Next, different hardening ratios, including 1%, 2%, 3%, 5%, 7.5%, 10%, and 15%, were considered in each analysis. Therefore, the ductility ratio of the bi-linear system, from $\mu = 2$ to $\mu = 8$, was determined using dynamic time history analysis. The ductility of the system was computed by maximum nonlinear displacement to yield displacement ratio using the irritative trial and error method to achieve constant ductility, where the lateral force decreases gradually until the ductility demand reaches to target ductility. The yield strength factor was determined at each constant-ductility ratio using $R = m.S_a/F_y$, where m is mass, S_a is the acceleration response spectrum at the desired period of vibration, and F_y is the yield strength of the system. In the end, the γ factor at each ductility, hardening ratio, soil type class, and period of vibration was determined by 352800 dynamic analyses regarding Eq. (3). The cited process for peak-oriented stiffness-strength deterioration hysteresis models was repeated, including modified Clough, moderate-stiffness-strength-deterioration, and severe-stiffness-strength-deterioration, as illustrated in Figs. 3(a) to (c). The peak-oriented models with different deterioration protocols are used to simulate the behavior of the reinforced concrete structures when subjected to cyclic loads. Several studies have shown that the amount of deterioration and stiffness loss in reinforced concrete specimens depends on the loading protocol and detailing of the steel bars, such as bar slippage. The uniaxial hysteresis material from the OpenSEES library was selected to model the hysteresis behavior of the concrete structures under SAC loading protocols to show different deteriorationregimes. Fig. 4 shows the entire procedure of the method.

3 Statistical analysis

As mentioned in the methodology section, the γ factor for seven hardening ratios, including 0% (EPP), 1%, 2%, 3%, 5%, 7.5%, 10%, and 15%, was computed in the period range of 0.1s to 3s. As shown in Fig. 5, the γ factor with different hardening ratios was normalized by the determined γ factor from the elastic-perfectly-plastic hysteresis model. Fig. 5 shows that the γ factor increases as the hardening ratio increases. Moreover, the effect of hardening increases by the growth of the ductility factor. Although the influence of lower hardening and ductility factors is not prominent, the consequence of higher hardening ratios and ductility in structures with a period of lower than 2 s is approximately more than 30 percent.

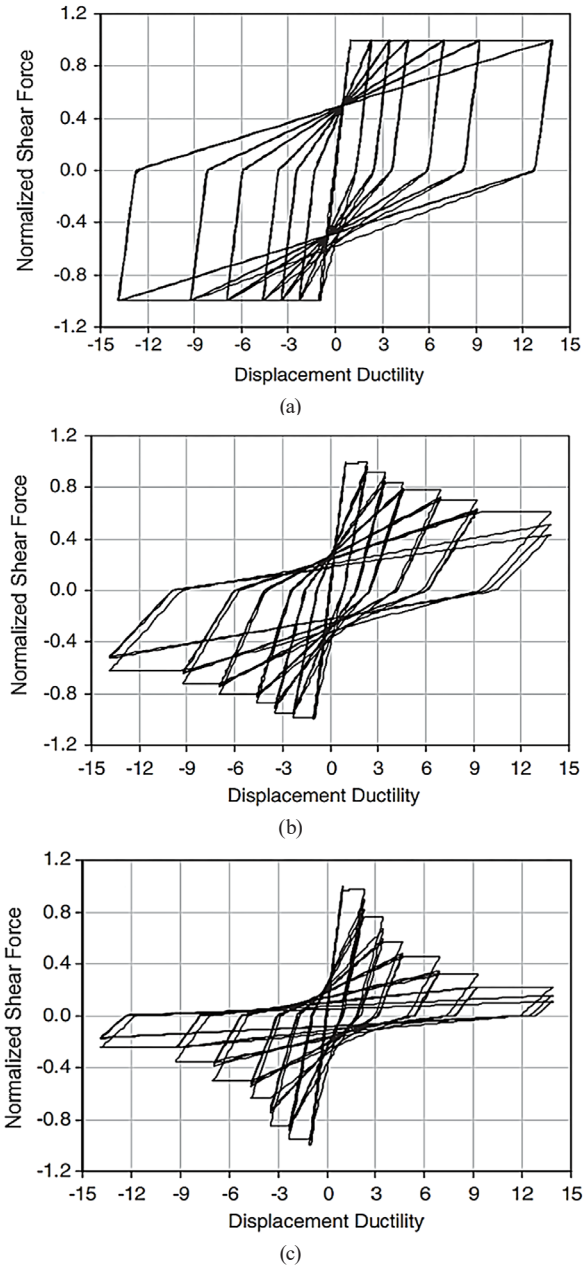

Fig. 3 Hysteresis deterioration models, (a) Modified Clough, (b) moderate-stiffness-strength-deterioration, (c) severe-stiffness-strength-deterioration

The effect of hardening on the γ factor is more prominent when the period of vibration is lower than 2 s. The following procedure was conducted for earthquake ground motions recorded on soil classes A, B, C, and D, based on Tables A1 to A3. As illustrated in Fig. 6, the effect of soil type for all classifications was evaluated by normalizing the γ factor determined from soil class C and D into the γ factor determined from soil class AB. Figs. 6(a) to (l) show that the effect of soil type in short-period regions (T < 0.5 s) is significant. Moreover, the influence of soil type increases as the ductility factor of the system increases. Additionally, the effect of soil type in long-period regions becomes significant by increasing system ductility. By comparing γ factors determined from recorded ground motions in different soil types, the influence of this parameter must be considered for estimating target displacement.

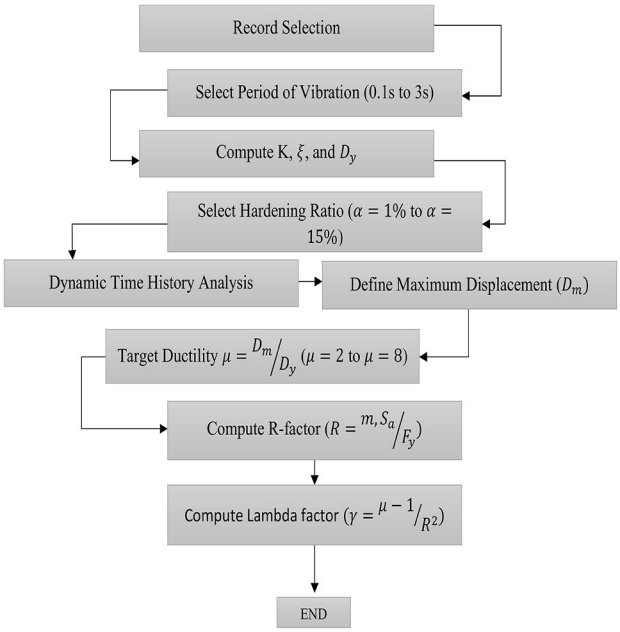

Fig. 4 Full procedure of methodology

The effect of stiffness-strength deterioration on the γ factor in different soil classes was investigated, according to Fig. 7. Figs. 7(a)–(c) shows the ratio of the γ factor determined from Modified Clough, moderate-stiffness-strength-deterioration, and severe-stiffness-strength-deterioration to EPP hysteresis model in soil class C group, respectively. As shown in Fig. 7, in the short period range, from 0.1 s to 1 s, the effect of stiffness-strength deterioration on the γ factor is additive and reduced by increasing the period of vibration. Instead of the short-period range, the influence of stiffness-strength-deterioration on the γ factor decreases with the increase of period in the long-period regions, but it remains constant. The effect of the ductility factor in stiffness-strength-deterioration hysteretic models is significant only in short to intermediate periods and increases by increasing the deterioration. The cited trend was observed in other soil classes. Hence, the influence of degradation on the γ factor must be considered for structural systems with deterioration mode.

A nonlinear equation was defined in Eq. (4) to compute the γ factor for different hardening ratios, soil class types, and deterioration protocols. Additionally, nonlinear regression analysis was performed to determine constant

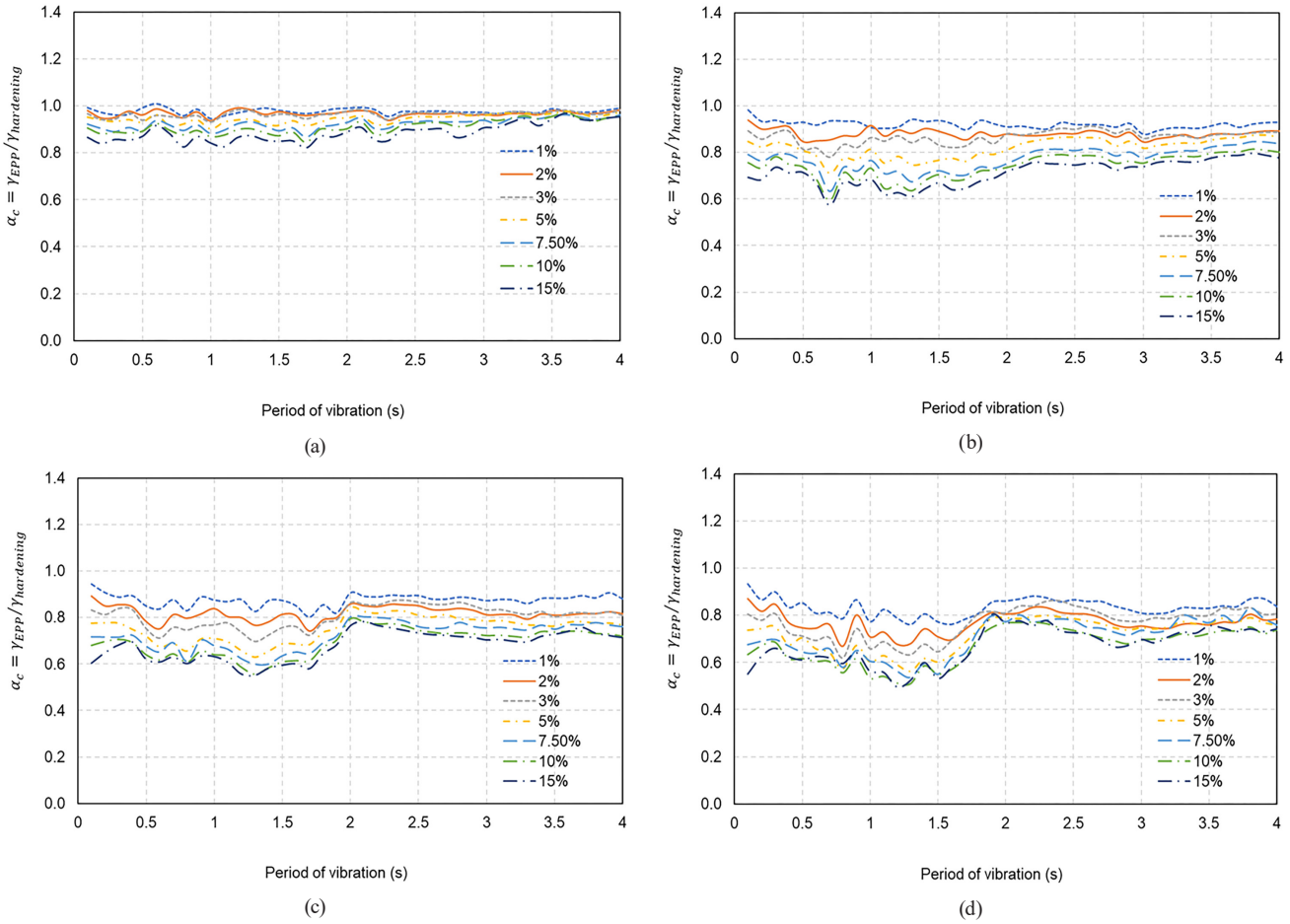

Fig. 5 The γ factor with bi-linear hardening hysteresis model to EPP hysteresis model, including (a) γ 22, (b) γ 44, (c) γ 66, (d) γ 8

regression parameters based on system ductility, hardening ratio, soil type, and stiffness-strength-deterioration. The suggested formula is given by:

$$\gamma = \alpha + \frac{(\mu - 1)^2}{\beta T^2}, \tag{4}$$

where μ is the ductility of the system, T is the fundamental period of vibration, and α, β are regression coefficients.

The Table C1 constant regression parameters can be used to estimate the γ factor based on ductility, hardening ratio, and soil class type. Moreover, Table C2 presents the constant regression parameters for Modified Clough, moderate-stiffness-strength-deterioration, and severe-stiffness-strength-deterioration models in different soil types and ductility ratios.

4 Verification of proposed method with designed models

In this study, four 1-, 3-, 7-, and 12-story steel moment structural buildings with different framing types were designed based on ASCE/SEI 7-16 [39] and AISC 360-16 [42] provisions to validate the proposed method in different period conditions. The 1- and 3-story structures were designed using ordinary and special moment framing systems (OMF and SMF), while the intermediate moment frame system (IMF) was used for 7- and 12-story models. The response modification factor (R), system overstrength (Ω), and deflection amplification factor (C_d) for 1- and 3-story structures were defined as 3.5, 3, 3, and 8, 3, 5.5, respectively. Additionally, the mentioned parameters were determined as 4.5, 3, and 4 for 7- and 12-story structures. The designed drift limit state was lower than 2.5% for 1- and 3-story structures and less than 2% for 7- and 12-story structural systems. In mentioned models, 3000 kg/m and 1000 kg/m dead and live load were considered in all designed models with the seismic load. The 5 m bay length and 3.5 m height were arbitrarily assumed in all models as a usual length in most buildings, where the total elevation in 1-, 3-, 7-, and 12-story models are 3.5 m, 10.5 m, 24.5 m, and 42 m, respectively. Structural sections in all models were designed under design seismic hazard level (DE) with 0.842 and 0.3795 spectral accelerations in short- (S_{SD}) and long-periods (S1D). The configuration


Soil class A, B
Soil class C
Soil class D
Hardening Ratio = 2%
Ductility = 2
$\gamma_{soil\ class}/\gamma_{soil\ class\ A,B}$
Period of vibration (s)

(a)


Soil class A, B
Soil class C
Soil class D
Hardening Ratio = 5%
Ductility = 2
$\gamma_{soil\ class}/\gamma_{soil\ class\ A,B}$
Period of vibration (s)

(b)

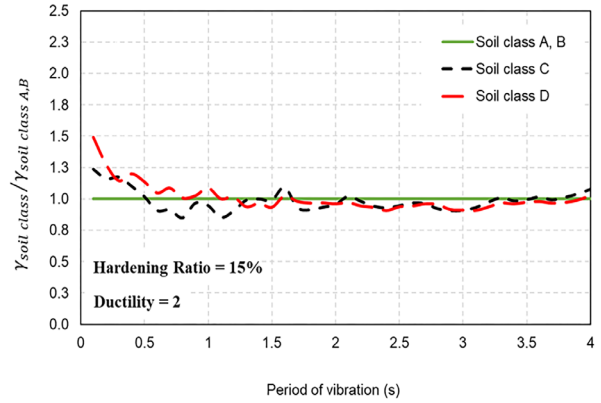
Soil class A, B
Soil class C
Soil class D
Hardening Ratio = 15%
Ductility = 2
$\gamma_{soil\ class}/\gamma_{soil\ class\ A,B}$
Period of vibration (s)

(c)

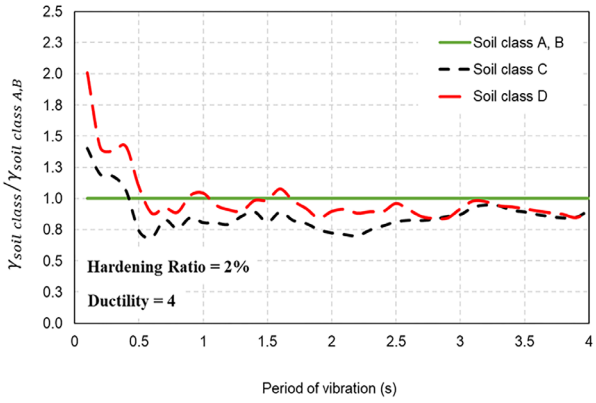
Soil class A, B
Soil class C
Soil class D
Hardening Ratio = 2%
Ductility = 4
$\gamma_{soil\ class}/\gamma_{soil\ class\ A,B}$
Period of vibration (s)

(d)


Soil class A, B
Soil class C
Soil class D
Hardening Ratio = 5%
Ductility = 4
$\gamma_{soil\ class}/\gamma_{soil\ class\ A,B}$
Period of vibration (s)

(e)

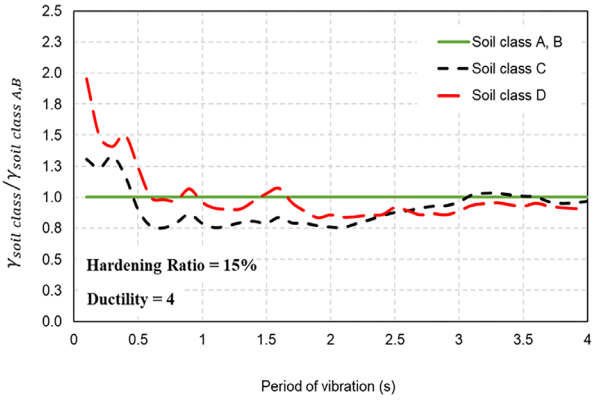
Soil class A, B
Soil class C
Soil class D
Hardening Ratio = 15%
Ductility = 4
$\gamma_{soil\ class}/\gamma_{soil\ class\ A,B}$
Period of vibration (s)

(f)

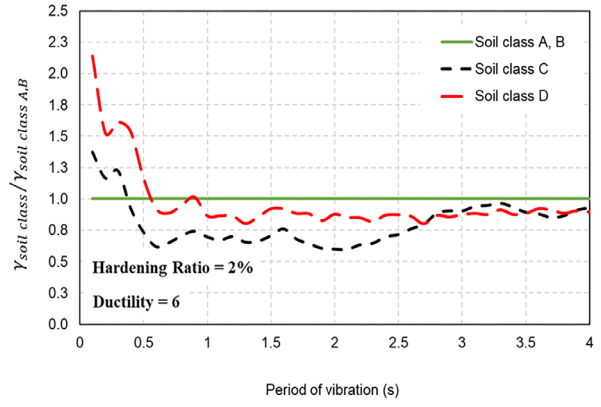
Soil class A, B
Soil class C
Soil class D
Hardening Ratio = 2%
Ductility = 6
$\gamma_{soil\ class}/\gamma_{soil\ class\ A,B}$
Period of vibration (s)

(g)

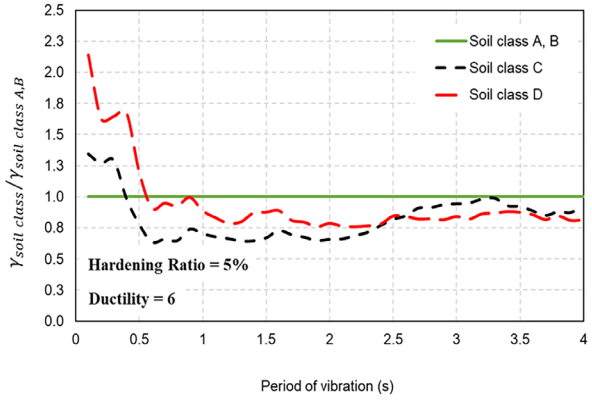
Soil class A, B
Soil class C
Soil class D
Hardening Ratio = 5%
Ductility = 6
$\gamma_{soil\ class}/\gamma_{soil\ class\ A,B}$
Period of vibration (s)

(h)

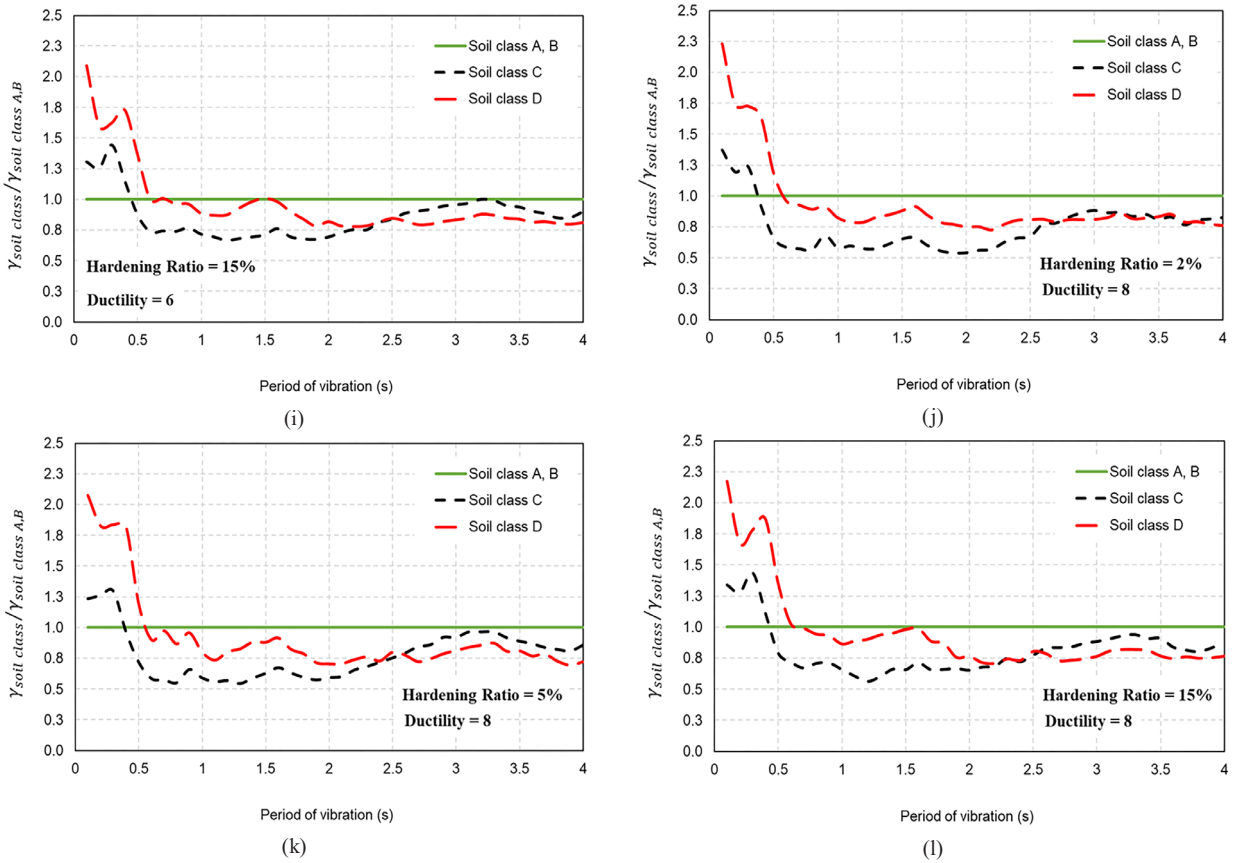

Fig. 6 The effect of soil classification on γ factor; (a) Ductility = 2, Hardening Ratio = 2%; (b) Ductility = 2, Hardening Ratio = 5%; (c) Ductility = 2, Hardening Ratio = 15%; (d) Ductility = 4, Hardening Ratio = 2%; (e) Ductility = 4, Hardening Ratio = 5%; (f) Ductility = 4, Hardening Ratio = 15%; (g) Ductility = 6, Hardening Ratio = 2%; (h) Ductility = 6, Hardening Ratio = 5%; (i) Ductility = 6, Hardening Ratio = 15%; (j) Ductility = 8, Hardening Ratio = 2%; (k) Ductility = 8, Hardening Ratio = 5%; (l) Ductility = 8, Hardening Ratio = 15%

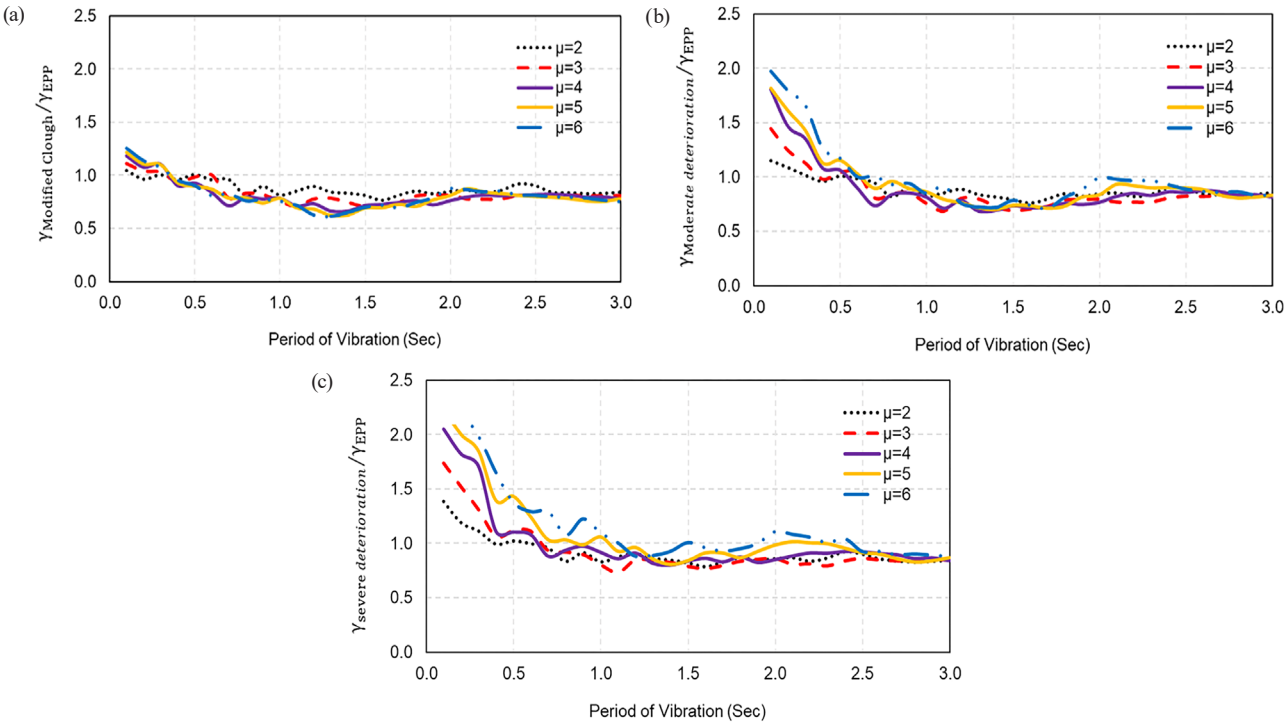

Fig. 7 The effect of stiffness-strength deterioration on γ factor for (a) Modified Clough, (b) moderate-stiffness-strength-deterioration, (c) severe-stiffness-strength-deterioration

of designed models and sections is illustrated in Fig. B1 in Appendix B. As shown in Fig. B1, the W-shape section with 2400 kg/cm^2 yield stress, 3700 kg/cm^2 ultimate stress, and 2000000 kg/cm^2 modules of elasticity was used for designed beams and columns. The target displacement for 1-, 3-, 7-, and 12-story structures were determined using dynamic time history analysis to validate the proposed methodology and formula. In the first step, the designed models were constructed in nonlinear Seismostruct V2021 software for fiber-based analysis under desired seismic hazard level. Hence, the 3D beam-column force-based element with five integration points along the members was used for fiber-based modeling (FBM). The fiber sections were divided into 150 mesh segments to attain accurate results. Secondly, the eigenvalue analysis was performed based on the mass and stiffness matrix to determine the period of vibration in different modes. The defined period of the system was used for scaling of selected ground motions, determining γ factor from Eq. (4), and using Rayleigh damping for time history analysis. The period of vibration in the first, second, and third vibration modes with higher effective modal participation for 1-, 3-, 7-, and 12-story structures are presented in Table 1.

In the third step, the pushover analysis based on ASCE/SEI 41-17 [1] was conducted to define pushover and idealized curves, as shown in Fig. 8. Moreover, the structural characteristics, including yield strength, yield displacement, system mass, effective stiffness, and hardening ratio, are presented in Table 2 (where F_y and D_y are yield strength and yield displacement, respectively). The roof displacement was selected as a controlling node for pushover analysis in all models. In the fourth step, the pushover capacity curves were converted to capacity energy curves (energy – displacement) by computing an area under force-displacement curves. In the fifth step, the higher seismic hazard level, higher than the designed level (DE level), was selected to evaluate target displacement in this hazard level. The cited seismic level was chosen to assess the designed structures in higher ductility values and nonlinearity. Then, the seismic hazard level (demand) was converted to the energy-displacement (energy demand) curve using Eqs. (5) and (6), respectively [8].

Table 1 Fundamental period of vibration in models

Modes	1-story	3- story	7-story	12-story
1th mode	0.335	1.279	1.938	3.064
2th mode	0.034	0.362	0.668	1.037
3th mode	0.034	0.176	0.378	0.607

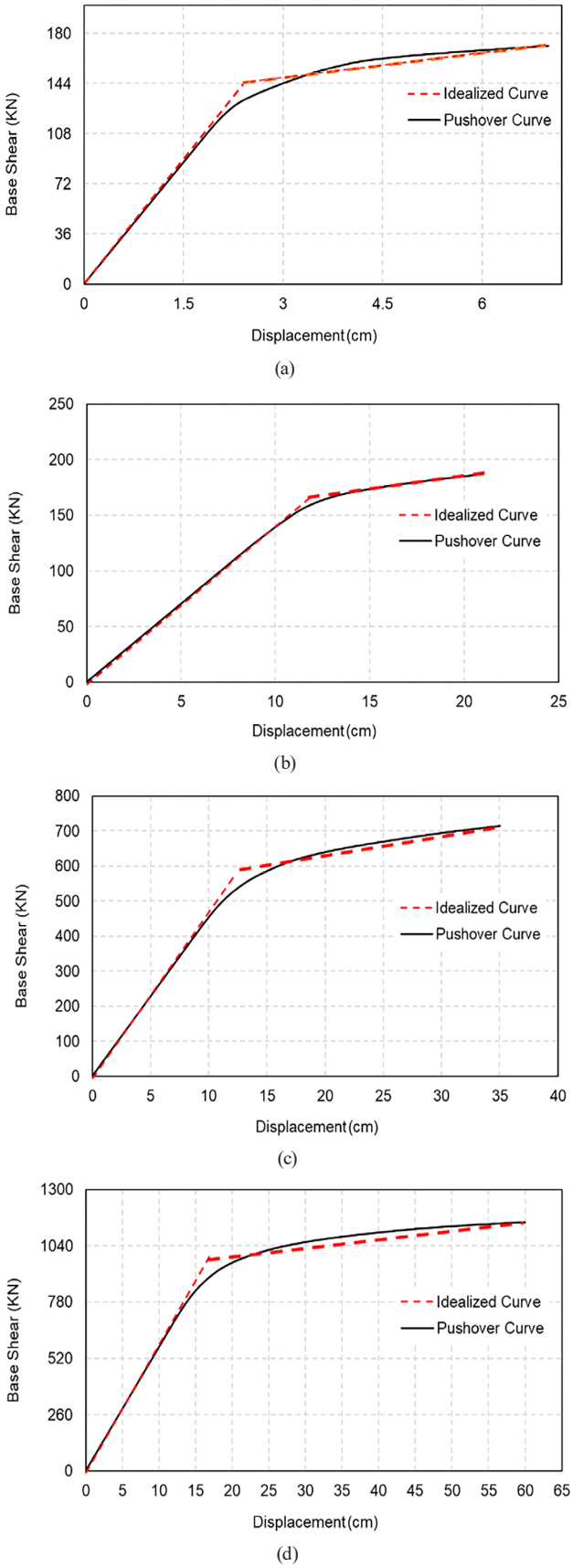

Fig. 8 Pushover and idealized curve for (a) 1-story, (b) 3-story, (c) 7-story, (d) 12-story

Table 2 Structural characteristics under pushover analysis

Models	F_y (KN)	D_y (cm)	Mass (kg)	Effective stiffness (N/m)	Hardening ratio
1-story	144	2.4	16710	6000000	14.5%
3-story	164	11.6	90626	1408513	15%
7-story	582	12.6	352854	4480000	13%
12-story	975	16.5	1011607	5850000	7.5%

$$E = \frac{1}{2} m \left(\frac{T}{2\pi} S_a \right)^2, \tag{5}$$

$$S_d = \frac{T^2}{4\pi^2} S_a, \tag{6}$$

where m is structural mass, T is fundamental period of vibration in the first mode, and S_a is acceleration spectrum.

In the sixth step, suitable earthquake ground motions were selected based on Baker and Lee's [40] algorithm from selected ground motions in Table A2. Recently, Amirchoupani et al. [35] proposed a new ground motion scaling method for better spectral matching of ground motions based on energy concepts. They showed that normalizing ground motions and scaling them regarding the fundamental period of vibration would lead to better spectral matching and lower error. In this method, the spectral response accelerations in sensitive-acceleration (if $0.05\ \text{s} < T < 0.5\ \text{s}$), sensitive-velocity (if $0.5\ \text{s} < T < 2.7\ \text{s}$), and sensitive-displacement regions (if $2.7\ \text{s} < T < 4\ \text{s}$) were normalized to acceleration spectrum intensity ($\int_{0.1}^{0.5} S_a(\zeta = 5\%, T)\,dT$), Housner intensity ($\int_{0.1}^{2.5} PSV(\zeta = 5\%, T)\,dT$), and peak ground displacement (PGD) firstly. It is worth mentioning that by normalizing response accelerations to pointed parameters, the normalizing index in the ground motions reaches one. Then, the scaling procedure based on ASCE/SEI 7 code would be performed as a next step. The mentioned method was used for ground motion scaling to decrease the error in predicting target displacement.

In the seventh step, according to the proposed equations in Section 3, the Gamma factor was computed based on the hardening ratio of structures, fundamental period of vibration, and ductility demand. Then, by intersecting capacity (energy pushover) and demand (energy hazard level) curves, the target displacement was determined at this point.

In the eighth step, the exact roof displacement extracted from nonlinear time history analysis was compared with the predicted roof displacement from the proposed equation and Leelataviwat et al. [7–9] estimation. Fig. 9 shows that the proposed method illustrates lower errors compared to exact responses extracted from fiber-based analytical models in the 1-story steel structure model. Generally, the estimation of responses in structures with short-period duration is accompanied by high variation due to the sensibility of nonlinear displacements in this region [34, 43, 44]. However, the mean error in the proposed method is about 10%, while the error in Goel et al. [45] and Leelataviwat et al. [7, 9] procedures is about 15%. It shows that the proposed method can estimate the target displacement suitably in short-period structures. Fig. 10 illustrates that the proposed method predicts the target displacement appropriately in middle-period structural systems. The predicted roof displacement is more pierce compared to exact values in the 3-story steel structure. The mean error in the proposed method is about 7%, while the mean error in the previous work is about 15%.

Fig. 11 shows that the mean error in the proposed method for the 7-story steel structure is about 6%, while the error in previous work compared to exact values is about 20%. It is concluded that the proposed method can estimate the

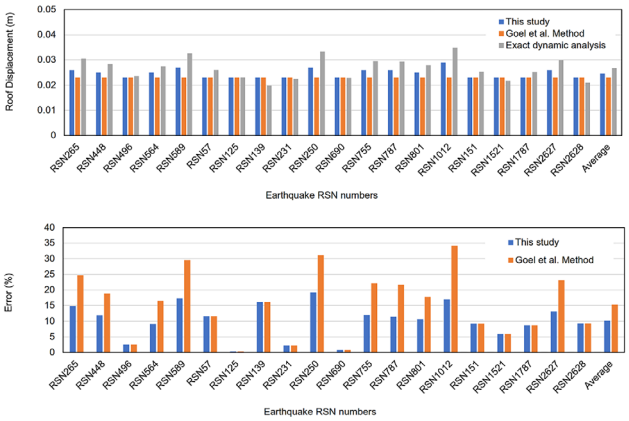

Fig. 9 Target roof displacement comparison between exact values, proposed formula, and Goel et al. study in 1-story steel structure

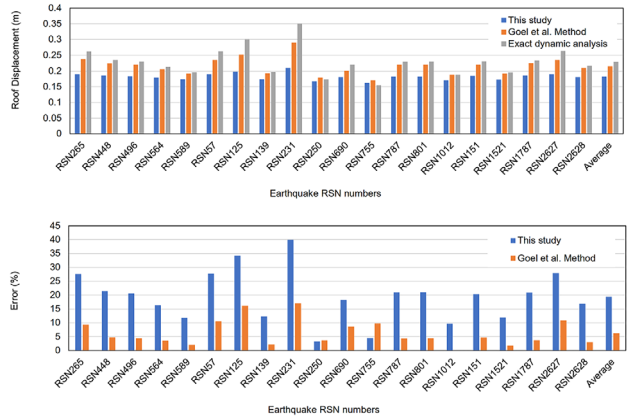

Fig. 10 Target roof displacement comparison between exact values, proposed formula, and Goel et al. study in 3-story steel structure

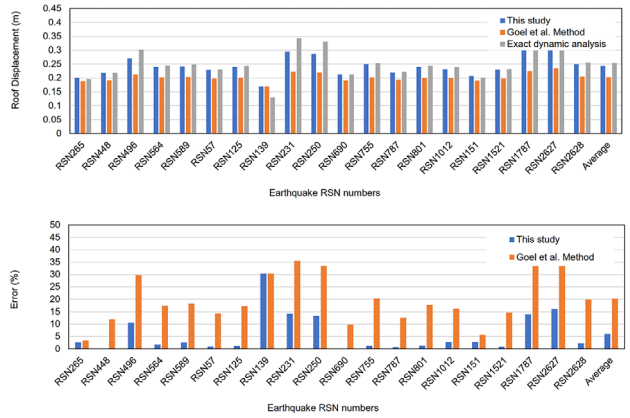

Fig. 11 Target roof displacement comparison between exact values, proposed formula, and Goel et al. [45] study in 7-story steel structure

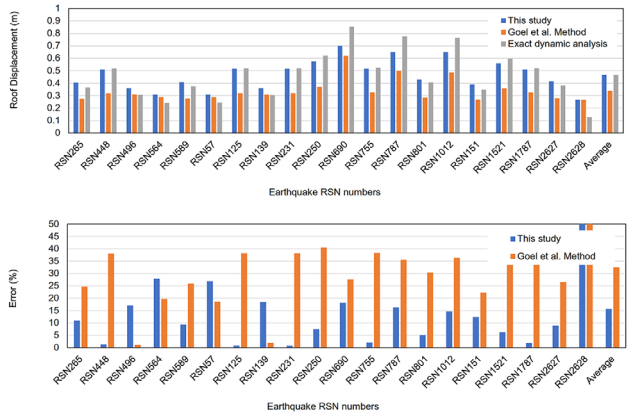

Fig. 12 Target roof displacement comparison between exact values, proposed formula, and Goel et al. study in 12-story steel structure

target displacement in high-rise structural systems with periods higher than 1.5 s. The mentioned procedure for the 12-story steel structure with a long-period duration was similarly repeated (higher than 3 s). As shown in Fig. 12, the mean error in the proposed method is about 16%, while the mean error in Goel et al. [45] and Leelataviwat et al. [7, 9] procedure is more than 30%. Hence, the proposed method and formula can evaluate target displacement in steel structural systems with a defined hardening ratio in the capacity curve, stiffness-strength-deterioration, and soil site condition.

5 Verification of proposed method with empirical RC bridge pier models

The empirical reinforced concrete (RC) bridge pier tested under uniaxial shake table analysis by Schoettler et al. [46] was considered to verify the proposed equation and procedure for the empirical RC model. The RC bridge pier was designed by Caltrans code specification [47] and constructed at the University of California (Berkeley), as illustrated in Fig. 13. The RC pier was tested using shake table analysis under sequential ground motions applied from low to high intensity to bring the RC pier near collapse. The ground motion characteristics are presented in Table 3. The 3D nonlinear beam-column element with five integration points along height was used for fiber-based modeling of the pier by Open System for Earthquake Engineering Simulation (OpenSEES) software. The Concrete02 [48] and reinforcing material from the OpenSEES library were adapted for numerical modeling of the unconfined (cover) and confined (core) parts of

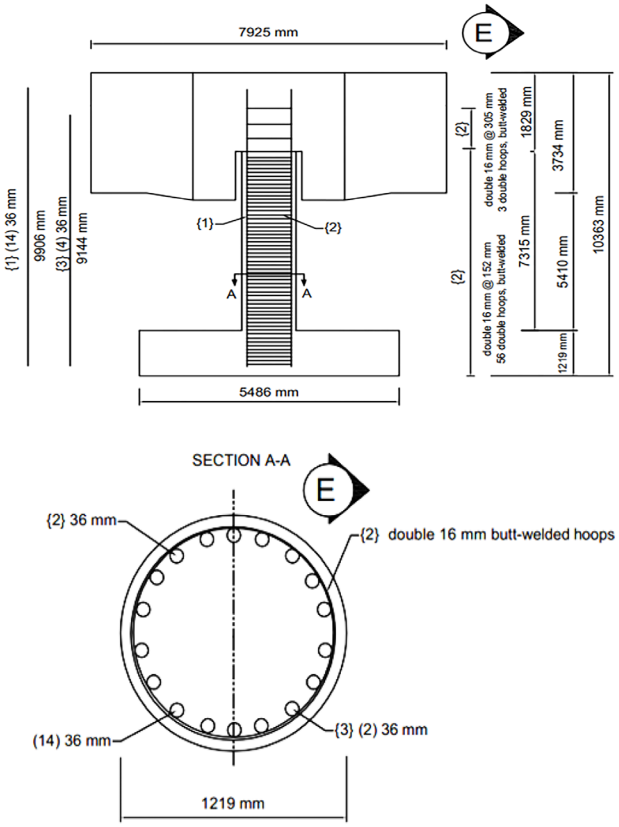

Fig. 13 Full-scale RC bridge pier specimen and cross-section [46]

Table 3 Ground motion characteristics for verification [46]

Test	Earthquake	M_w	Station	Comp.	Sc	PGA (g)
EQ1	1989 Loma Prieta	6.9	Agnew	90	1	-0.199
EQ2	1989 Loma Prieta	6.9	Corralitos	90	1	0.409
EQ3	1989 Loma Prieta	6.9	LGPC	0	1	0.526
EQ4	1989 Loma Prieta	6.9	Corralitos	90	1	0.454
EQ5	1995 Kobe	6.9	Takatori	0	-0.8	-0.533
EQ6	1989 Loma Prieta	6.9	LGPC	0	1	-0.512

the section and steel bars, respectively. Accordingly, the Coffin-Manson equation was assumed to take into account the mechanical effect of strain softening, low-cycle fatigue, transition from elastic behavior to inelastic, and compressive buckling (the $\alpha = 0.506$, $C_f = 0.361$, $C_d = 0.6$ was used in Coffin-Manson model). Table 4 presents the pier characteristics used in the RC model, including column dimensions and material strengths. The RC pier section was divided into 150 mesh elements in different integration points to achieve accurate results (Fig. 14(a)).

The bond-slip behavior was employed by considering a zero-length element to model the member end rotation according to the strain penetration between the RC pier (superstructure) and foundation to compute moment-curvature responses, as shown in Figs. 14(b) to (c). Hence, six parameters were defined to capture the bond-slip effect in the connection between elements, as discussed by Zhao and Sritharan [49] based on Fig. 14(c).

The S_y and S_u were computed by Eqs. (7) and (8), given as:

$$S_y = 2.54\left[\frac{d_b}{8437}\frac{F_y}{\sqrt{f_c}}(2\alpha+1)\right]^{1/\alpha} + 0.34\,, \tag{7}$$

$$S_u = 30 \sim 40 S_y\,, \tag{8}$$

where d_b is rebar diameter, f_c is the compressive strength of concrete, F_y is yield strength (MPa), α is the constant parameter taken as 0.4 based on CEB-FIP model code 90, and b is initial hardening ratio in the monotonic slip versus bar responses ($S_y = 0.548$, $S_u = 19.18$, $b = 0.4$, $R = 0.75$ parameters were used in model).

Table 4 Material properties and pier dimensions [24, 46]

Parameters	Values
Column diameters (m)	1.22
Column height (m)	7.32
Concrete cover (mm)	50
Longitudinal reinforcement diameter (mm)	18 Φ 35.8
Yield stress (MPa)	519
Ultimate stress (MPa)	707
Initial elastic tangent (MPa)	196000
Tangent at initial strain hardening (MPa)	5520
Strain corresponding to initial strain hardening (%)	1.1
Strain at peak stress (%)	12.2
Transverse reinforcement diameter (mm)	15.9 @ 152
Yield stress (MPa)	338
Ultimate stress (MPa)	592
Strain at peak stress (%)	12.5
Axial load (MN)	2.32

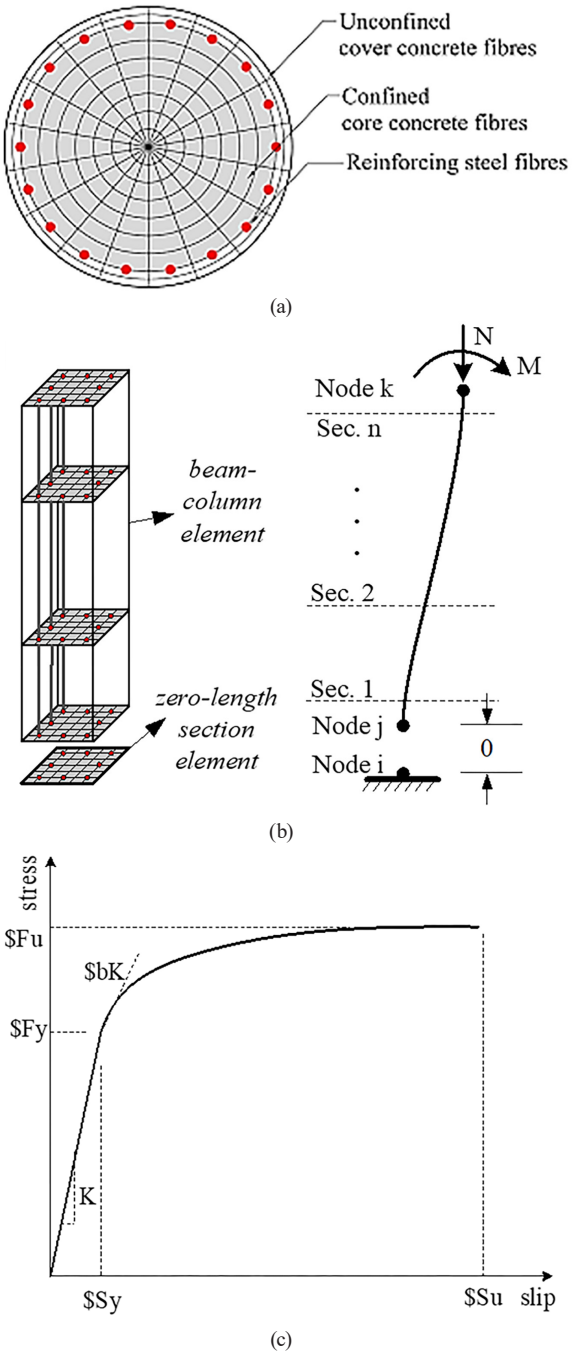

Fig. 14 (a) Fiber section model, (b) Distribution of plastic hinge with bond-slip behavior, (c) Uniaxial bond-slip material [49]

Fig. 15 shows the appropriate verification between empirical and numerical models under sequential ground motions presented in Table 3.

The mentioned procedure in Section 4 was repeated for the RC bridge pier, including eigenvalue analysis, pushover analysis, conversion from V_b–D_t to E–D_t, and dynamic time history analysis. It is worth mentioning that the fundamental period of vibration in the RC bridge pier is 0.61 seconds based on its stiffness and mass. Fig. 16

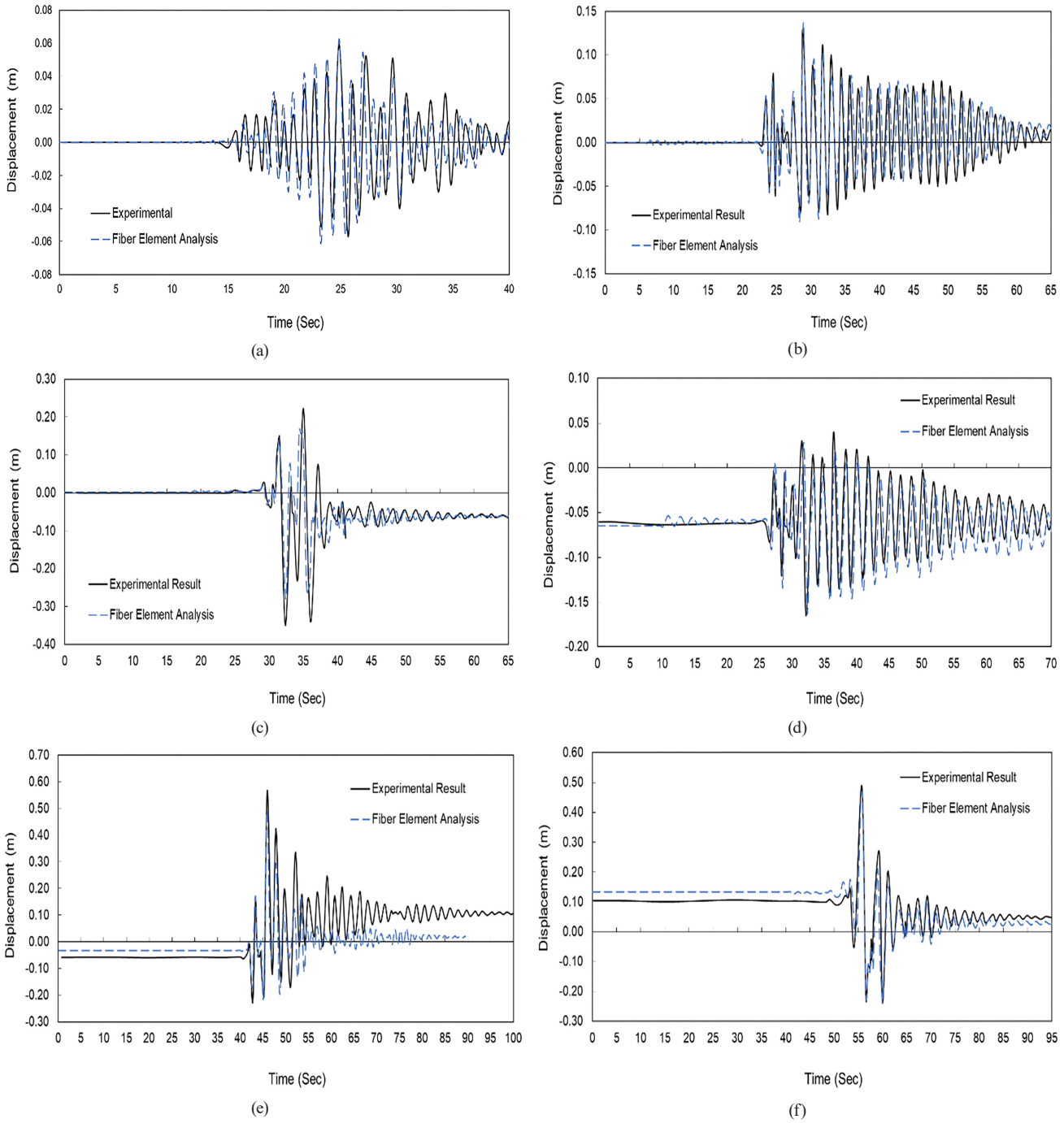

Fig. 15 Verification between empirical shake table analysis and numerical fiber-based model; (a) EQ1, (b) EQ2, (c) EQ3, (d) EQ4, (e) EQ5, (f) EQ6

indicates the pushover analysis of the RC bridge pier under the monotonic load pattern and its idealized curve, where the yield displacement, yield force, and ultimate displacement is 7.5 (cm), 700 (KN), and 60 (cm), respectively.

Table 5 illustrates the comparison between obtained responses from the nonlinear time history analysis and calculated ones from the approximated equation in this study. Accordingly, the proposed method estimates the target displacement of the RC bridge pier appropriately compared with the previous investigation. It is necessary to explain that the presented result was somewhat predictable because the past results were only valid for the steel structures.

Fig. 17 illustrates the intersection of input energy demand and capacity energy determined by the proposed method in this investigation and previous studies to estimate the target displacement of the empirical RC bridge

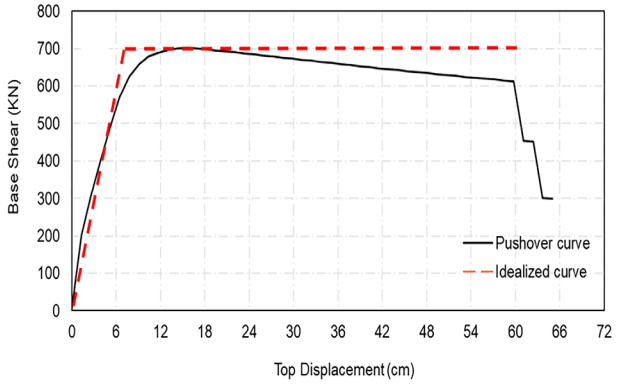

Fig. 16 Pushover analysis on empirical RC bridge pier

pier. It should be noted that the mentioned figure presents for better understanding, whereas the other comparisons are available in Table 5. Fig. 17 indicates that the approximate proposed method is more accurate for estimating target displacement compared to obtained displacements from time history analysis.

6 Conclusion

The γ factor in different hardening ratios, stiffness-strength-deterioration approaches, and soil type classes was determined in this investigation to predict the target displacement in structural systems with various configurations. Hence, the following results were obtained:

- The effect of hardening on the γ factor increases as the ductility of the system increases.
- The influence of the hardening ratios on the γ factor in $T < 2$ s was prominent.
- The effect of soil type class on the γ factor increases as the ductility of the system increases.
- The influence of soil type class in short-period regions is significant, while this effect increases in the long-period area by increasing the ductility.
- The effect of the stiffness-strength-deterioration hysteresis models on the γ factor is considerable, especially in $T < 1$ s.
- As the deterioration increases, the γ factor increases in $T < 1$ s and decreases in $T > 1$ s. These effects amplify in higher ductility.
- A simple formula based on ductility, hardening ratio, strength-stiffness-deterioration regimes, soil condition, and period of vibration was suggested to predict target displacement in different structures.

Table 5 The comparison between obtained responses from the nonlinear time history analysis and calculated ones from the approximated equation in this study and previous studies

Records	D_{max}	$D_{max(Goel)}$	D_{THA}	μ_u	Error	$Error_{(Goel)}$
RSN265	0.11	0.093	0.12	1.6	8	22
RSN448	0.14	0.094	0.16	2.1	16	41
RSN496	0.14	0.095	0.17	2.2	16	42
RSN564	0.09	0.093	0.08	1.1	7	11
RSN589	0.13	0.093	0.15	1.9	10	36
RSN57	0.11	0.093	0.12	1.6	8	23
RSN125	0.13	0.094	0.16	2.1	18	41
RSN139	0.11	0.093	0.11	1.4	1	12
RSN231	0.12	0.093	0.13	1.7	7	28
RSN250	0.12	0.093	0.13	1.7	8	28
RSN690	0.14	0.096	0.18	2.4	21	46
RSN755	0.13	0.093	0.15	1.9	10	36
RSN787	0.12	0.093	0.13	1.7	7	28
RSN801	0.11	0.093	0.12	1.6	11	24
RSN1012	0.12	0.093	0.14	1.8	12	32
RSN1512	0.12	0.093	0.14	1.8	12	32
RSN1521	0.11	0.093	0.11	1.4	2	13
RSN1787	0.15	0.1	0.20	2.7	27	50
RSN2627	0.15	0.1	0.20	2.6	26	49
RSN2628	0.10	0.093	0.09	1.2	10	2
Average	0.12	0.09405	0.14	1.8	12	30

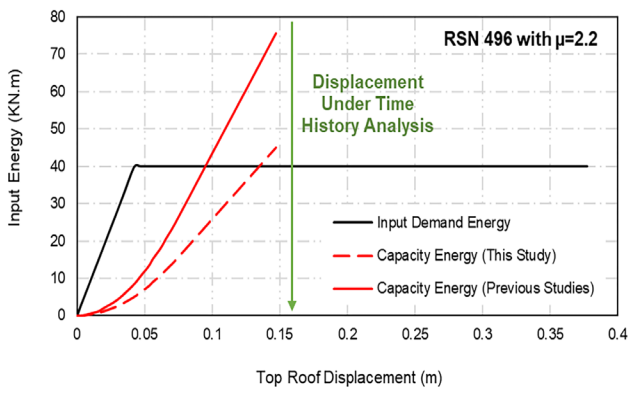

(a)

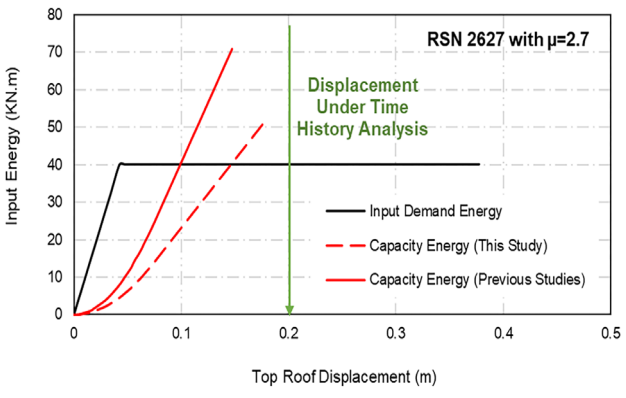

(b)

Fig. 17 The top roof displacement of RC bridge pier using energy balance method under proposed method; (a) RSN 496, (b) RSN 2627

- The direct nonlinear time history analysis using fiber-based models, including 1-, 3-, 7-, and 12-story steel moment systems, were compared with Goel et al. [45], Leelataviwat et al. [7, 9], and approximate equation of this study. Statistical results showed that the mean error based on previous data in estimating target displacement for 1-, 3-. 7-, and 12-story structures was about 15%, 20%, 20%, and 32%, respectively. Conversely, the mean error in this study for estimating target displacement of 1-, 3-. 7-, and 12-story structures was about 10%, 7%, 6%, 15%, respectively.
- The applicability of the proposed equation was examined on an empirical RC bridge pier with the appropriate estimation of target responses and minimum error.

References

[1] ASCE "ASCE/SEI 41-17, Seismic evaluation and retrofit of existing buildings", American Society of Civil Engineers, Reston, VA, USA, 2017. https://doi.org/10.1061/9780784414859

[2] ATC "ATC-40, Seismic evaluation and retrofit of concrete buildings", Applied Technology Council, Redwood City, CA, USA, Rep. SSC 96-01, 1996.

[3] Fajfar, P. "A nonlinear analysis method for performance-based seismic design", Earthquake Spectra, 16(3), pp. 573–592, 2000. https://doi.org/10.1193/1.1586128

[4] Kreslin, M., Fajfar, P. "The extended N2 method considering higher mode effects in both plan and elevation", Bulletin of Earthquake Engineering, 10, pp. 695–715, 2012. https://doi.org/10.1007/s10518-011-9319-6

[5] Lee, S.-S., Goel, S. C. "Performance-Based Design of Steel Moment Frames using Target Drift and Yield Mechanism", University of Michigan, Ann Arbor, MI, USA, Rep. UMCEE 01-17, 2001.

[6] Leelataviwat, S., Goel, S. C., Stojadinović, B. "Toward performance-based seismic design of structures", Earthquake Spectra, 15(3), pp. 435–461, 1999. https://doi.org/10.1193/1.1586052

[7] Leelataviwat, S., Saewon, W., Goel, S. C. "An energy based method for seismic evaluation of structures", In: Proceedings of Structural Engineers Association of California Convention SEAOC 2007, Lake Tahoe, CA, USA, Sep, 26-29, 2007, pp. 21–37.

[8] Leelataviwat, S., Goel, S. C., Stojadinović, B. "Energy-based seismic design of structures using yield mechanism and target drift", Journal of Structural Engineering, 128(8), pp. 1046–1054, 2002. https://doi.org/10.1061/(ASCE)0733-9445(2002)128:8(1046)

[9] Leelataviwat, S., Saewon, W., Goel, S. C. "Application of Energy Balance Concept in Seismic Evaluation of Structures", Journal of Structural Engineering, 135(2), pp. 113–121, 2009. https://doi.org/10.1061/(asce)0733-9445(2009)135:2(113)

[10] Xiong, E.-G., He, H., Cui, F.-F., Bai, L. "Performance-Based Plastic Design Method for Steel Concentrically Braced Frames Using Target Drift and Yield Mechanism", Periodica Polytechnica Civil Engineering, 60(1), pp. 127–134, 2016. https://doi.org/10.3311/PPci.7383

[11] Shoeibi, S., Kafi, M. A., Gholhaki, M. "Performance-Based Seismic Design and Parametric Assessment of Linked Column Frame System", Periodica Polytechnica Civil Engineering, 62(3), pp. 555–569, 2018. https://doi.org/10.3311/PPci.10920

[12] Borekci, M., Kirçil, M. S., Ekiz, I. "Inelastic Displacement Ratios for Evaluation of Degrading Peak – Oriented SDOF Systems", Periodica Polytechnica Civil Engineering, 62(1), pp. 33–47, 2018. https://doi.org/10.3311/PPci.10635

[13] Veletsos, A. S., Newmark, N. M., Chelapati, C. V. "Deformation Spectra for Elastic and Elastoplastic Systems Subjected to Ground Shock and Earthquake Motions", In: Proceedings of the 3rd World Conference on Earthquake Engineering, Auckland, Wellington, New Zealand, 1965, pp. II-663-II-682.

[14] Veletsos, A., Newmark, N. M. "Effect of inelastic behavior on the response of simple systems to earthquake motions", In: Proceedings of the 2nd World Conference on Earthquake Engineering, Tokyo, Kyoto, Japan, 1960, pp. 895–912.

[15] Miranda, E. "Seismic evaluation and upgrading of existing structures", PhD thesis, University of California at Berkeley, 1991.

[16] Miranda, E. "Evaluation of site-dependent inelastic seismic design spectra", Journal of Structural Engineering, 119(5), pp. 1319–1338, 1993. https://doi.org/10.1061/(ASCE)0733-9445(1993)119:5(1319)

[17] Miranda, E. "Estimation of inelastic deformation demands of SDOF systems", Journal of Structural Engineering, 127(9), pp. 1005–1012, 2001. https://doi.org/10.1061/(ASCE)0733-9445(2001)127:9(1005)

[18] Baez, J. I., Miranda, E. "Amplification Factors to Estimate Inelastic Displacement Demands for the Design of Structures in the Near Field", In: Proceedings of 12th World Conference on Earthquake Engineering, Auckland, New Zealand, 2000, pp. 1–8. ISBN: 9780958215435

[19] Ruiz-García, J., Miranda, E. "Inelastic displacement ratios for design of structures on soft soils sites", Journal of Structural Engineering, 130(12), pp. 2051–2061, 2004. https://doi.org/10.1061/(ASCE)0733-9445(2004)130:12(2051)

[20] Iwan, W. D. "Estimating inelastic response spectra from elastic spectra", Earthquake Engineering & Structural Dynamics, 8(4), pp. 375–388, 1980. https://doi.org/10.1002/eqe.4290080407

[21] Rosenblueth, E., Herrera, I. "On a kind of hysteretic damping", Journal of the Engineering Mechanics Division, 90(4), pp. 37–48, 1964. https://doi.org/10.1061/JMCEA3.0000510

[22] Gulkan, P., Sozen, M. A. "Inelastic responses of reinforced concrete structure to earthquake motions", ACI Journal Proceedings, 71(12), pp. 604–610, 1974.

[23] Newmark, N. M., Hall, W. J. "Earthquake spectra and design", Engineering Monographs on Earthquake Criteria, University of California, Berkley, CA, USA, 1982. ISBN: 0-943198-22-4

[24] Amirchoupani, P., Abdollahzadeh, G., Hamidi, H. "Improvement of energy damage index bounds for circular reinforced concrete bridge piers under dynamic analysis", Structural Concrete, 22(6), pp. 3315–3335, 2021.
https://doi.org/10.1002/suco.202000762

[25] Zhang, R., Wang, W., Ke, K. "Quantification of seismic demands of damage-control tension-only concentrically braced steel beam-through frames (TCBSBFs) subjected to near-fault ground motions based on the energy factor", Soil Dynamics and Earthquake Engineering, 129, 105910, 2020.
https://doi.org/10.1016/j.soildyn.2019.105910

[26] Ke, K., Chuan, G., Ke, S. "Seismic energy factor of self-centering systems subjected to near-fault earthquake ground motions", Soil Dynamics and Earthquake Engineering, 84, pp. 169–173, 2016.
https://doi.org/10.1016/j.soildyn.2016.02.011

[27] Ke, K., Yam, M. C. H. "Energy-factor-based damage-control evaluation of steel MRF systems with fuses", Steel and Composite Structures, 22(3), pp. 589–611, 2016.
https://doi.org/10.12989/scs.2016.22.3.589

[28] Ke, K., Yam, M. C. H. "A performance-based damage-control design procedure of hybrid steel MRFs with EDBs", Journal of Constructional Steel Research, 143, pp. 46–61, 2018.
https://doi.org/10.1016/j.jcsr.2017.12.011

[29] Wang, F., Ke, K., Zhang, H., Yam, M. C. H. "Constant-ductility-based energy factor demands of oscillators with modified Clough hysteretic model", Soil Dynamics and Earthquake Engineering, 115, pp. 36–40, 2018.
https://doi.org/10.1016/j.soildyn.2018.08.014

[30] Bida, Z., Fulong, L., Chengqing, L., Xianhong, W., Zhenzhe, H., Ke, L. "Hysteretic behavior of CHS X-joints under in-plane bending moment", Structures, 43, pp. 1790–1806, 2022.
https://doi.org/10.1016/j.istruc.2022.07.006

[31] Zhao, B., Sun, C., Cai, Y., Liu, C. "An out-of-plane bending hysteretic model for multi-planar CHS X-connections", Structures, 23, pp. 335–350, 2020.
https://doi.org/10.1016/j.istruc.2019.10.003

[32] Ruiz-García, J., Miranda, E. "Inelastic displacement ratios for evaluation of structures built on soft soil sites", Earthquake Engineering & Structural Dynamics, 35(6), pp. 679–694, 2006.
https://doi.org/10.1002/eqe.552

[33] Rahnama, M., Krawinkler, H. "Effect of soft soils and hysteresis models on seismic design spectra", Stanford University, Stanford, CA, USA, Rep. 108, 1993.

[34] Amirchoupani, P., Abdollahzadeh, G., Hamidi, H. "Development of inelastic displacement ratio using constant energy-based damage index for performance-based design", Bulletin of Earthquake Engineering, 21, pp. 3461–3491, 2023.
https://doi.org/10.1007/s10518-023-01652-8

[35] Amirchoupani, P., Abdollahzadeh, G., Hamidi, H. "Spectral acceleration matching procedure with respect to normalization approach", Bulletin of Earthquake Engineering, 18(11), pp. 5165–5191, 2020.
https://doi.org/10.1007/s10518-020-00897-x

[36] Abdollahzadeh, G., Pourkalhor, S., Vakhideh, A., Pourbahram, Z., Amirchoupani, P. "Quantifying the optimal time gap between consecutive events", Asian Journal of Civil Engineering, 24, pp. 1373–1392, 2023.
https://doi.org/10.1007/s42107-023-00575-8

[37] FEMA 356, "Prestandard and commentary for the seismic rehabilitation of buildings", Federal Emergency Management Agency, Washington, DC, USA, 2000.

[38] FEMA 440, "Improvement of Nonlinear Static Seismic Analysis Procedures", Federal Emergency Management Agency, Washington, DC, USA, 2005.

[39] ASCE/SEI 7-16, "Minimum Design Loads and Associated Criteria for Buildings and Other Structures", American Society of Civil Engineers, Reston VA, USA, 2016.

[40] Baker, J. W., Lee, C. "An Improved Algorithm for Selecting Ground Motions to Match a Conditional Spectrum", Journal of Earthquake Engineering, 22(4), pp. 708–723, 2018.
https://doi.org/10.1080/13632469.2016.1264334

[41] Miranda, E. "Inelastic displacement ratios for structures on firm sites", Journal of Structural Engineering, 126(10), pp. 1150–1159, 2000.
https://doi.org/10.1061/(ASCE)0733-9445(2000)126:10(1150)

[42] AISC 360-16, "Specification for Structural Steel Buildings", American Institute of Steel Construction, Chicago, IL, USA, 2016.

[43] Ruiz-García, J., Miranda, E. "Probabilistic estimation of maximum inelastic displacement demands for performance-based design", Earthquake Engineering & Structural Dynamics, 36(9), pp. 1235–1254, 2007.
https://doi.org/10.1002/eqe.680

[44] Miranda, E., Bertero, V. V. "Evaluation of strength reduction factors for earthquake-resistant design", Earthquake Spectra, 10(2), pp. 357–379, 1994.
https://doi.org/10.1193/1.1585778

[45] Goel, S. C., Liao, W.-C., Bayat, M. R., Chao, S.-H. "Performance-based plastic design (PBPD) method for earthquake-resistant structures: An overview", Structural Design of Tall and Special Buildings, 19(1–2), pp. 115–137, 2010.
https://doi.org/10.1002/tal.547

[46] Schoettler, M. J., Restrepo, J. I., Guerrini, G., Duck, D. E., Carrea, F. "A full-scale, single-column bridge bent tested by shake-table excitation. PEER report 2015/02. Pacific Earthquake Engineering Research Center (PEER)", University of California, Berkeley, CA, 2015.

[47] California Department of Transportation "Caltrans seismic design criteria", Ver. 1.6, 2010. [online] Available at: https://dot.ca.gov/programs/engineering-services/

[48] Kent, D. C., Park, R. "Flexural members with confined concrete", Journal of the Structural Division, 97(7), pp. 1969–1990, 1971.

[49] Zhao, J., Sritharan, S. "Modeling of strain penetration effects in fiber-based analysis of reinforced concrete structures", ACI Structural Journal, 104(2), pp. 133–141, 2007.
https://doi.org/10.14359/18525

Appendix A

Table A1 Soil class A, B earthquake ground motions

NO	RSN	Year	Earthquake Name	Station Name	M_w	Mechanism	R_{jb} (km)	R_{rup} (km)	V_{s30} (m/sec)
1	80	1971	San Fernando	Pasadena	6.6	Reverse	21.5	21.5	969.07
2	146	1979	Coyote Lake	Gilroy Array #1	5.7	strike slip	10.21	10.67	1428.14
3	455	1984	Morgan Hill	Gilroy Array #1	6.1	strike slip	14.9	14.91	1428.14
4	680	1987	Whittier Narrows	Pasadena	5.9	Reverse Oblique	6.78	18.12	969.07
5	703	1987	Whittier Narrows	Vasquez Rocks Park	5.9	Reverse Oblique	47.25	50.39	996.43
6	765	1989	Loma Prieta	Gilroy Array #1	6.9	Reverse Oblique	8.84	9.64	1428.14
7	788	1989	Loma Prieta	Piedmont Jr High Sch.	6.9	Reverse Oblique	72.9	73	895.36
8	789	1989	Loma Prieta	Point Bonita	6.9	Reverse Oblique	83.37	83.45	1315.92
9	795	1989	Loma Prieta	SF-Pacific Heights	6.9	Reverse Oblique	75.96	76.05	1249.86
10	797	1989	Loma Prieta	SF-Rincon Hill	6.9	Reverse Oblique	74.04	74.14	873.1
11	804	1989	Loma Prieta	So. San Francisco	6.9	Reverse Oblique	63.03	63.15	1020.62
12	1011	1994	Northridge	LA-Wonderland Ave	6.6	Reverse	15.11	20.29	1222.52
13	1091	1994	Northridge	Vasquez Rocks Park	6.6	Reverse	23.1	23.64	996.43
14	1108	1995	Kobe	Kobe University	6.9	strike slip	0.9	0.92	1043
15	1613	1999	Duzce	Lamont 1060	7.1	strike slip	25.78	25.88	782
16	1649	1991	Sierra Madre	Vasquez Rocks Park	5.6	Reverse	37.63	39.81	996.43
17	2753	1999	Chi-Chi	CHY102	6.2	strike slip	39.3	39.32	804.36
18	2989	1999	Chi-Chi	CHY102	6.2	Reverse	69.76	74.16	804.36
19	3251	1999	Chi-Chi	TTN042	6.2	Reverse	84.68	85.17	845.34
20	3925	2000	Tottori	OKYH07	6.6	strike slip	15.23	15.23	940.2
21	3954	2000	Tottori	SMNH10	6.6	strike slip	15.58	15.59	967.27
22	4083	2004	Parkfield	PARKFIELD	6.0	strike slip	4.66	5.29	906.96
23	4167	2004	Niigata	FKSH07	6.6	Reverse	52.15	52.3	828.95
24	4312	1984	Umbria	Gubbio	5.6	Normal	14.67	15.72	922
25	5483	2008	Iwate	AKTH05	6.9	Reverse	37.45	39.41	829.46
26	5618	2008	Iwate	IWT010	6.9	Reverse	16.26	16.27	825.83
27	5646	2008	Iwate	IWTH14	6.9	Reverse	99.04	99.05	816.31
28	5649	2008	Iwate	IWTH17	6.9	Reverse	72.44	72.44	1269.78
29	5650	2008	Iwate	IWTH18	6.9	Reverse	64.27	64.27	891.55
30	5655	2008	Iwate	IWTH23	6.9	Reverse	68.03	68.03	922.89
31	5670	2008	Iwate	MYG011	6.9	Reverse	82.93	82.93	1423.8
32	5679	2008	Iwate	MYGH03	6.9	Reverse	56.72	56.72	933.96
33	5680	2008	Iwate	MYGH04	6.9	Reverse	40.42	40.43	849.83
34	5685	2008	Iwate	MYGH11	6.9	Reverse	57.15	57.15	859.19
35	8167	2003	San Simeon	Diablo Canyon.	6.5	Reverse	37.92	37.97	1100

Table A2 Soil class C earthquake ground motions

NO	RSN	Year	Earthquake Name	Station Name	M_w	Mechanism	R_{jb} (km)	R_{rup} (km)	V_{s30} (m/sec)
1	57	1971	San Fernando	Castaic-Old Ridge Route	6.6	Reverse	19.33	22.63	450.28
2	125	1976	Friuli	Tolmezzo	6.5	Reverse	14.97	15.82	505.23
3	139	1978	Tabas	Dayhook	7.3	Reverse	0	13.94	471.53
4	231	1980	Mammoth Lakes	Long Valley Dam	6.0	Normal Oblique	12.56	15.46	537.16
5	250	1980	Mammoth Lakes	Long Valley Dam	5.9	strike slip	9.65	16.03	537.16
6	265	1980	Victoria	Cerro Prieto	6.3	strike slip	13.8	14.37	471.53
7	448	1984	Morgan Hill	Anderson Dam	6.1	strike slip	3.22	3.26	488.77
8	496	1985	Nahanni	Site 2	6.7	Reverse	0	4.93	605.04
9	564	1986	Kalamata	Kalamata	6.2	Normal	6.45	6.45	382.21
10	589	1987	Whittier Narrows	Alhambra-Fremont School	5.9	Reverse Oblique	1.67	14.66	549.75
11	690	1987	Whittier Narrows	San Gabriel-E Grand Ave	5.9	Reverse Oblique	0	15.2	401.37
12	755	1989	Loma Prieta	Coyote Lake Dam	6.9	Reverse Oblique	19.97	20.34	561.43
13	787	1989	Loma Prieta	Palo Alto - SLAC Lab	6.9	Reverse Oblique	30.62	30.86	425.3
14	801	1989	Loma Prieta	San Jose - Santa Teresa Hills	6.9	Reverse Oblique	14.18	14.69	671.77
15	1012	1994	Northridge	LA 00	6.6	Reverse	9.87	19.07	706.22
16	1512	1999	Chi-Chi	TCU078	7.6	Reverse Oblique	0	8.2	443.04
17	1521	1999	Chi-Chi	TCU089	7.6	Reverse Oblique	0	9	671.52
18	1787	1999	Hector Mine	Hector	7.1	strike slip	10.35	11.66	726
19	2627	1999	Chi-Chi	TCU076	6.2	Reverse	13.04	14.66	614.98
20	2628	1999	Chi-Chi	TCU078	6.2	Reverse	0	7.62	443.04
21	4031	2003	San Simeon	Templeton-1-story Hospital	6.5	Reverse	5.07	6.22	410.66
22	4130	2004	Parkfield-02	Parkfield-Vineyard Cany 1E	6.0	strike slip	1.59	2.96	381.27
23	4141	2004	Parkfield-02	PARKFIELD - UPSAR 05	6.0	strike slip	9.14	9.61	440.59
24	4143	2004	Parkfield-02	PARKFIELD - UPSAR 07	6.0	strike slip	9.14	9.61	440.59
25	4147	2004	Parkfield-02	PARKFIELD - UPSAR 11	6.0	strike slip	8.93	9.41	466.12
26	4213	2004	Niigata	NIG023	6.6	Reverse	25.33	25.82	654.76
27	4229	2004	Niigata	NIGH12	6.6	Reverse	9.93	10.72	564.25
28	4481	2009	L'Aquila	L'Aquila-V. Aterno	6.3	Normal	0	6.81	685
29	4846	2007	Chuetsu-oki	Joetsu Yanagishima paddocks	6.8	Reverse	28.07	31.43	605.71
30	4864	2007	Chuetsu-oki	Yoitamachi Yoita Nagaoka	6.8	Reverse	4.69	16.1	655.45
31	4873	2007	Chuetsu-oki	Kashiwazaki City	6.8	Reverse	10.38	20.03	561.59
32	5286	2007	Chuetsu-oki	NIGH13	6.8	Reverse	29.84	33.57	461.1
33	5478	2008	Iwate	AKT023	6.9	Reverse	11.68	16.96	555.96
34	5656	2008	Iwate	IWTH24	6.9	Reverse	3.1	5.18	486.41
35	8486	2004	Parkfield-02	Hog Canyon	6.0	strike slip	4.51	5.28	376

Table A3 Soil class D earthquake ground motions

NO	RSN	Year	Earthquake Name	Station Name	M_w	Mechanism	R_{jb} (km)	R_{rup} (km)	V_{s30} (m/sec)
1	95	1972	Managua	Managua-ESSO	6.24	strike slip	3.51	4.06	288.77
2	174	1979	Imperial Valley	El Centro Array #11	6.53	strike slip	12.56	12.56	196.25
3	183	1979	Imperial Valley	El Centro Array #8	6.53	strike slip	3.86	3.86	206.08
4	322	1983	Coalinga	Cantua Creek School	6.36	Reverse	23.78	24.02	274.73
5	367	1983	Coalinga	Pleasant Valley P.P. - bldg	6.36	Reverse	7.69	8.41	257.38
6	614	1987	Whittier Narrows	Downey – Birchdale	5.99	Reverse Oblique	14.9	20.79	245.06
7	700	1987	Whittier Narrows	Tarzana - Cedar Hill	5.99	Reverse Oblique	38.24	41.22	257.21
8	725	1987	Superstition Hills	Poe Road (temp)	6.54	strike slip	11.16	11.16	316.64
9	776	1989	Loma Prieta	Hollister - South & Pine	6.93	Reverse Oblique	27.67	27.93	282.14
10	778	1989	Loma Prieta	Hollister Differential Array	6.93	Reverse Oblique	24.52	24.82	215.54
11	783	1989	Loma Prieta	Oakland - Outer Harbor Wharf	6.93	Reverse Oblique	74.16	74.26	248.62
12	799	1989	Loma Prieta	SF Intern. Airport	6.93	Reverse Oblique	58.52	58.65	190.14
13	848	1992	Landers	Coolwater	7.28	strike slip	19.74	19.74	352.98
14	949	1994	Northridge	Arleta - Nordhoff Fire Sta	6.69	Reverse	3.3	8.66	297.71
15	995	1994	Northridge	LA - Hollywood Stor FF	6.69	Reverse	19.73	24.03	316.46
16	998	1994	Northridge	LA - N Westmoreland	6.69	Reverse	23.4	26.73	315.06
17	999	1994	Northridge	LA - Obregon Park	6.69	Reverse	35.43	37.36	349.43
18	1082	1994	Northridge	Sun Valley - Roscoe Blvd	6.69	Reverse	5.59	10.05	320.93
19	1101	1995	Kobe	Amagasaki	6.9	strike slip	11.34	11.34	256
20	1141	1995	Dinar	Dinar	6.4	Normal	0	3.36	219.75
21	3749	1992	Cape Mendocino	Fortuna Fire Station	7.01	Reverse	16.54	20.41	355.18
22	4108	2004	Parkfield	Parkfield - Fault Zone 3	6	strike slip	1.1	2.73	211.74
23	4112	2004	Parkfield	Parkfield - Fault Zone 8	6	strike slip	3.05	3.95	308.84
24	4207	2004	Niigata	NIG017	6.63	Reverse	4.22	12.81	274.17
25	4861	2007	Chuetsu-oki	Nakanoshima Nagaoka	6.8	Reverse	10.73	19.89	319
26	4866	2007	Chuetsu-oki	Kawanishi Izumozaki	6.8	Reverse	0	11.75	338.32
27	4875	2007	Chuetsu-oki	Kariwa	6.8	Reverse	0	12	282.57
28	4896	2007	Chuetsu-oki	Kashiwazaki NPP	6.8	Reverse	0	10.97	201
29	5664	2008	Iwate	MYG005	6.9	Reverse	10.71	13.47	361.24
30	5814	2008	Iwate	Furukawa Osaki City	6.9	Reverse	31.07	31.08	248.19
31	5836	2010	El Mayor	El Centro - Meloland Geot.	7.2	strike slip	28.53	29	264.57
32	6877	1992	Joshua Tree	Indio - Jackson Road	6.1	strike slip	25.04	25.53	292.12
33	6893	2010	Darfield	DFHS	7	strike slip	11.86	11.86	344.02
34	6923	2010	Darfield	Kaiapoi North School	7	strike slip	30.53	30.53	255
35	8067	2011	Christchurch	Christchurch Cashmere High Sc	6.2	Reverse Oblique	4.44	4.46	204

Appendix B

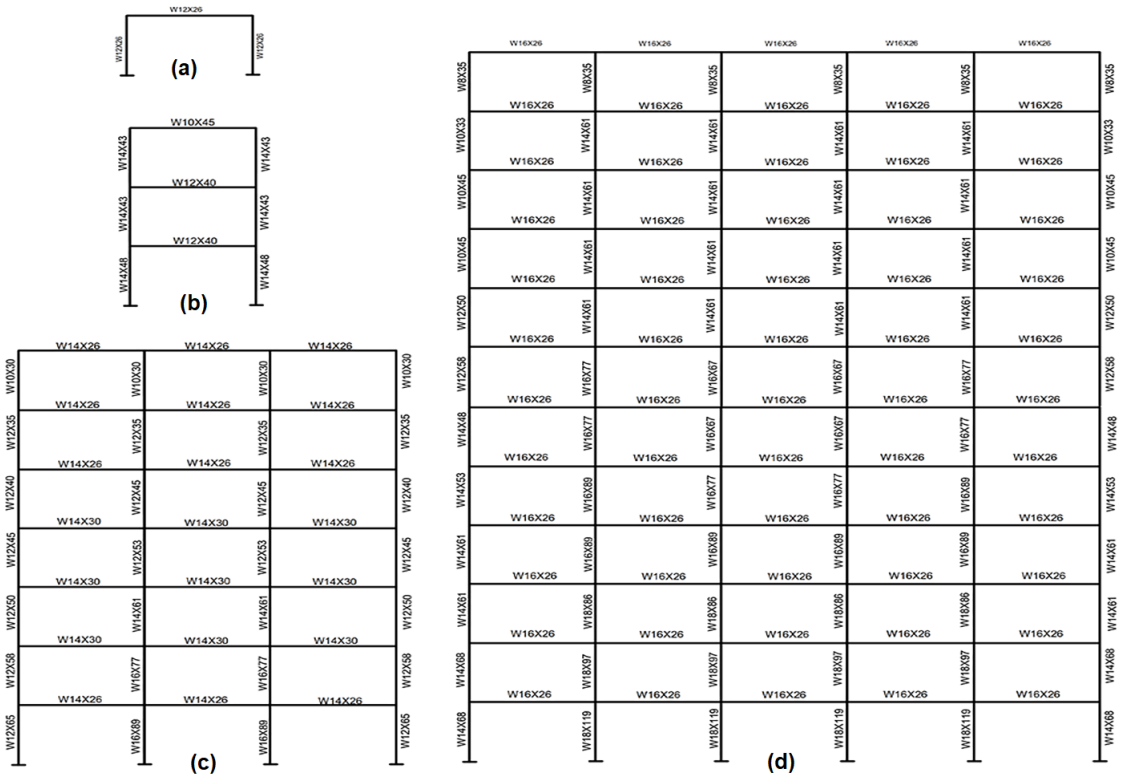

Fig. B1 The configuration of designed (a) 1-story, (b) 3-story, (c) 7-story, (d) 12-story models

Appendix C

Table C1 Constant regression parameters (α, β) based on ductility, hardening ratio, and soil type

Hardening ratio – Soil class A, B														
Ductility	1%		2%		3%		5%		7.5%		10%		15%	
	α	β	α	β	α	β	α	β	α	β	α	β	α	β
2	0.66	256	0.65	265	0.65	267	0.63	287	0.62	309	0.61	322	0.59	436
3	0.56	623	0.55	638	0.54	651	0.51	713	0.49	759	0.49	1507	0.44	7013
4	0.50	1001	0.48	1143	0.47	1085	0.43	1204	0.41	1285	0.39	1346	0.37	2030
5	0.46	1529	0.43	1537	0.42	1667	0.38	1786	0.36	1842	0.34	2011	0.32	1583
6	0.43	2111	0.39	2096	0.38	2228	0.35	2117	0.32	2528	0.31	2743	0.31	2896
8	0.37	3017	0.34	3308	0.33	3418	0.30	3668	0.29	4224	0.18	2926	0.27	5812
Hardening ratio – Soil class C														
Ductility	1%		2%		3%		5%		7.5%		10%		15%	
	α	β	α	β	α	β	α	β	α	β	α	β	α	β
2	0.63	146	0.63	149	0.62	154	0.60	153	0.59	161	0.58	164	0.55	74
3	0.49	343	0.48	352	0.47	367	0.45	378	0.43	400	0.41	412	0.37	265
4	0.40	563	0.38	591	0.38	638	0.35	664	0.33	708	0.31	746	0.30	661
5	0.34	840	0.32	885	0.31	955	0.29	1020	0.27	1096	0.26	1155	0.26	2678
6	0.29	1152	0.27	1225	0.27	1339	0.25	1441	0.24	1558	0.23	1646	0.23	1991
8	0.23	1911	0.21	2068	0.21	2311	0.19	2504	0.19	2727	0.18	2926	0.19	3317

Continuation of Table C1

Hardening ratio – Soil class D														
Ductility	1%		2%		3%		5%		7.5%		10%		15%	
	α	β	α	β	α	β	α	β	α	β	α	β	α	β
2	0.65	111	0.65	109	0.64	110	0.63	113	0.61	115	0.60	117	0.58	122
3	0.54	237	0.52	235	0.51	241	0.48	247	0.45	253	0.44	264	0.41	288
4	0.47	382	0.44	385	0.42	394	0.39	411	0.36	425	0.35	447	0.34	496
5	0.41	541	0.38	553	0.36	561	0.33	594	0.31	623	0.30	662	0.28	749
6	0.36	720	0.34	727	0.31	753	0.28	796	0.27	853	0.26	908	0.27	1118
8	0.30	1102	0.27	1118	0.25	1170	0.23	1267	0.22	1365	0.22	1487	0.21	1801

Table C2 Constant regression parameters (α, β) based on ductility, deterioration status, and soil type

Hardening ratio – Soil class A, B						
Ductility	MD		MSD		SSD	
	α	β	α	β	α	β
2	0.62	174.4	0.64	58.27	0.65	40.58
3	0.53	358.6	0.57	109.6	0.6	74.22
4	0.49	542.8	0.54	170	0.58	117
5	0.46	791.6	0.53	236	0.58	175.4
6	0.44	1025	0.49	275.8	0.56	203.2
Hardening ratio – Soil class C						
Ductility	MD		MSD		SSD	
	α	β	α	β	α	β
2	0.54	39.43	0.54	40.1	0.54	34.4
3	0.39	122.46	0.39	97.46	0.41	77.72
4	0.32	235.3	0.32	168.4	0.36	139.6
5	0.27	383.5	0.29	257.2	0.32	195.3
6	0.24	572.3	0.26	357	0.30	260.7
Hardening ratio – Soil class D						
Ductility	MD		MSD		SSD	
	α	β	α	β	α	β
2	0.58	42.46	0.58	37.31	0.59	33.53
3	0.46	96.64	0.47	81.24	0.49	64.92
4	0.39	162.12	0.41	122	0.43	100.24
5	0.34	240.3	0.36	167.5	0.39	128.57
6	0.31	321.7	0.33	228.1	0.36	173.1